*Progress In Electromagnetics Research, Vol. 160, 9–17, 2017*

# General Near Field Synthesis of Reflectarray Antennas for Their Use as Probes in CATR

**Daniel R. Prado*, Álvaro F. Vaquero, Manuel Arrebola, Marcos R. Pino, and Fernando Las-Heras**

**Abstract**—In this work, reflectarray antennas are proposed for their use as probes in compact antenna test ranges. For that purpose, the quiet zone generated by a single offset reflectarray is enhanced, overcoming the limitation imposed by the amplitude taper of the feed antenna. First, the near field is characterized by a radiation model which computes the near field of the reflectarray as far field contributions of each element, which are modeled as small rectangular apertures and thus taking into account the active element pattern. Then, a phase only synthesis is performed with the Levenberg-Marquardt algorithm in order to improve the size of the generated quiet zone. Due to the nature of the application, this near field synthesis takes into account both the amplitude and phase, making it a more challenging task than an amplitude-only synthesis. The optimization is focused on flattening the amplitude while trying to preserve the phase front generated by the reflectarray.

## 1. INTRODUCTION

Reflectarray antennas are most commonly used in far field applications [1], such as Direct Broadcast Satellite (DBS) [2–5], Local Multipoint Distribution Service (LMDS) [6–8] or radar interferometers [9, 10]; while near field applications are less conventional. Nevertheless, in recent years reflectarrays have been proposed in near field for Radio-Frequency IDentification (RFID) reader applications [11], imaging [12] or microwave virus sanitizer [13]. One near field application which remains uncharted by reflectarrays is Compact Antenna Test Ranges (CATR) [14], which employ one or more parabolic reflectors to simulate open range conditions in a closed environment, so the far field of the antenna under test can be directly measured. This is done thanks to the properties of the parabolic reflector, which collimates the field coming from the focus where the feed is placed, generating a volume in front of the antenna known as quiet zone, which complies with certain requirements both in amplitude and phase, with a maximum allowable ripple (typically 10° in phase and 1 dB in amplitude) [14]. However, CATR systems based on parabolic reflectors have some drawbacks, such that the parabolic reflectors are bulky and expensive to fabricate, especially at high frequencies where the required surface error must be very low [14, 15]. In this regard, printed planar reflectarrays may be a potential candidate for CATR systems in high frequency bands, since they are based on the microstrip technology and thus are low profile, are easy and low cost to manufacture, while keeping good agreement with simulations [1]. Furthermore, this kind of antenna has been demonstrated at 94 GHz [16], with manufacturing errors in the printed elements which are lower than $\pm 1\,\mu$m, and should allow to manufacture reflectarrays in the frequency range from 100 GHz to 200 GHz maintaining good accordance between measurements and simulations, provided a good electromagnetic model.

*Received 27 July 2017, Accepted 7 October 2017, Scheduled 25 October 2017*

* Corresponding author: Daniel Rodriguez Prado (drprado@tsc.uniovi.es).
The authors are with the Department of Electrical Engineering, Group of Signal Theory and Communications, Universidad de Oviedo, Gijón 33203, Spain.

A parametric study of the quiet zone generated by conventional reflectarray antennas was carried out in [17], where the critical parameters that limit the size of the quiet zone were identified. Later, in [18] a technique for the optimization of the near field amplitude was presented. The goal was to flatten the amplitude in several near field planes for applications such as RFID tag identification or femto cell coverage for cellular systems. Limited results were obtained in [19] in the synthesis of the complex near field.

In this work, reflectarray antennas are proposed as potential candidates as probes for CATR systems. First, a model for the computation of the reflectarray near field, which takes into account the active element pattern, is proposed and validated through the use of commercial software GRASP. The model computes the near field as contribution of far fields from all the reflectarray elements. This model is then employed in a near field Phase-Only Synthesis (POS) to improve the quiet zone generated by the reflectarray antenna. The chosen algorithm is the Levenberg-Marquardt (LMA), which has been effectively used in array synthesis with success [20–27], and it takes into account both amplitude and phase of the near field, since CATR requirements impose a maximum allowable ripple in both, making it a more challenging task than an amplitude-only synthesis. The optimization is performed in several near field planes, flattening the amplitude and phase, greatly improving the size of the quiet zone. In contrast to previous works in the literature [19], the synthesis is improved by considering a circular coverage zone which adapts better to the taper imposed by the feed, as well as limiting the amplitude of the near field outside the coverage zone, avoiding losing power to regions outside the area of interest. Finally, the proposed framework for general near field optimization may be employed for other applications, such as near field (multi-)focusing, by providing the desired specifications via an appropriate template and setting the near field phase cost function to zero. Furthermore, it can also be extended to far field applications by substituting the near field model by a far field one.

## 2. REFLECTARRAY NEAR FIELD MODEL

### 2.1. Reflectarray Near Field

Reflectarray antennas are able to collimate the field wave coming from the feed at any given direction by properly choosing the phase-shift introduced by its elements [1]. This way, a planar phase front can be generated in front of the antenna. However, the size of the quiet zone will be limited in amplitude due to the strong taper imposed by the feed. This fact was checked by near-field measurements of a prototype [28] in a planar range [29]. The measured reflectarray is squared, formed by 1080 elements in a regular grid of $36 \times 30$, with periodicity $5\,\text{mm} \times 6\,\text{mm}$ and was designed to radiate a pencil beam. The feed is a K-band standard pyramidal horn from Narda working at 20 GHz and placed at $(-85, 0, 180)$ mm in

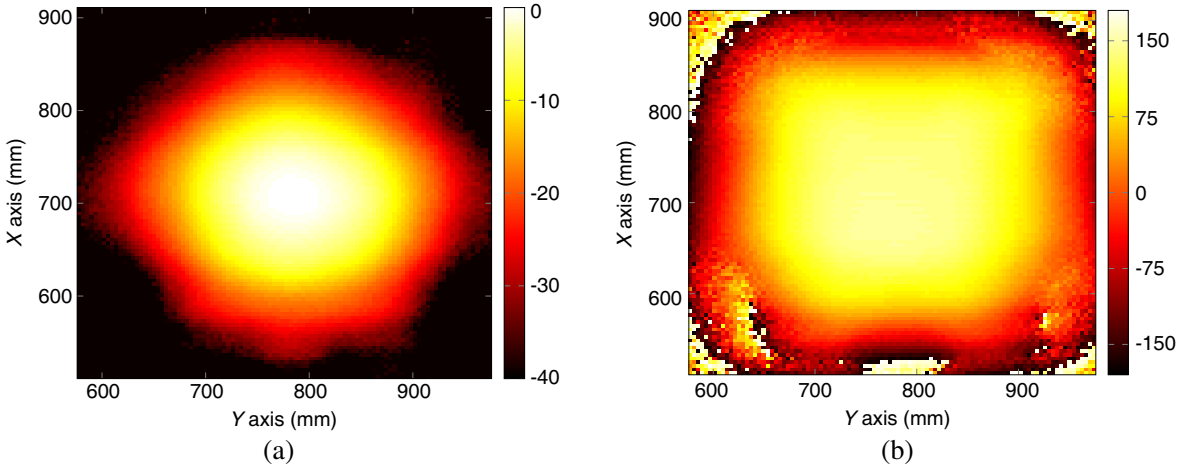


**Figure 1.** Near field measurements at 20 GHz on a plane $26.67\lambda$ away from the reflectarray center. (a) Amplitude (dB). (b) Phase (degrees).

the reflectarray coordinate system. The unit cell is comprised of two layers of stacked patches, employing a commercial substrate CuClad 233LX with $\varepsilon_r = 2.33$, $\tan\delta = 0.0012$ and thickness 0.787 mm. Both layers are bonded with a bonding film with $\varepsilon_r = 2.32$, $\tan\delta = 0.0012$ and thickness 0.037 mm.

Figure 1 shows the measurement in amplitude and phase at a plane $26.67\lambda$ away from the reflectarray center. The values of the $X$ and $Y$ axis correspond to the placement of the antenna in the measurement setup coordinate system [29]. The shape of the amplitude is due to the illumination taper of the feed in the surface of the reflectarray. The phase measurement clearly shows the phase front with the shape of the antenna aperture. In both images, some interferences can be seen for lower values of $X$ which are produced by the supporting structure and horn. As reference, the most restrictive main cuts have a quiet zone size of $3.3\lambda \times 2.9\lambda$ and $6.0\lambda \times 5.3\lambda$ in amplitude and phase, respectively. From these results, it is clear that in order to employ a reflectarray antenna as a probe for CATR applications, a near field synthesis must be performed in order to increase the size of the quiet zone in amplitude, while maintaining the phase front.

### 2.2. Near Field Model

In order to compute the near field of the single-offset reflectarray antenna depicted in Figure 2, we propose a model in which the unit radiation element is the unit cell of the antenna, considering it a small rectangular aperture (instead of a punctual, isotropic source) in which the field is constant. Then, the near field of the reflectarray at each point in space will be computed as contribution of the far field radiated by all the elements of the reflectarray.

The far field radiated by each cell is computed using the Second Principle of Equivalence considering the tangential field constant. In spherical coordinates it takes the form

$$\begin{aligned} E_\theta^{X/Y} &= \frac{jk}{2\pi r} e^{-jkr} \left( P_{x,mn}^{X/Y} \cos\varphi + P_{y,mn}^{X/Y} \sin\varphi \right), \\ E_\varphi^{X/Y} &= -\frac{jk}{2\pi r} e^{-jkr} \cos\theta \left( P_{x,mn}^{X/Y} \sin\varphi - P_{y,mn}^{X/Y} \cos\varphi \right), \end{aligned} \tag{1}$$

where $P_{x,mn}^{X/Y}$ and $P_{y,mn}^{X/Y}$ are the spectrum functions for each $(m,n)$ reflectarray element. For the unit cell, considering $E_{\mathrm{ref},mn}^{X/Y}$ its constant tangential field for either component $x$ or $y$ and $(a,b)$ the periodicity, they take the form

$$P_{mn}^{X/Y} = E_{\mathrm{ref},mn}^{X/Y} ab \,\mathrm{sinc}\left(\frac{k_0 ua}{2}\right) \mathrm{sinc}\left(\frac{k_0 vb}{2}\right), \tag{2}$$

where $u = \sin\theta\cos\varphi$ and $v = \sin\theta\sin\varphi$ are the usual spherical coordinates. Eq. (2) is the Fourier transform of the tangential field on the reflectarray element and accounts for the active element pattern.

Since the near field is calculated as contributions of far fields, it will be valid when it is obtained at least at far field distance of the reflectarray element, which is $2\lambda$ for a periodicity of $0.5\lambda$ [30]; and it is also in the Fresnel region of the whole reflectarray. In addition, the distance at which the near field is computed must be $z > z_f$ to avoid direct radiation from the feed (see Figure 2). In general, this last imposition would suffice since it usually includes the other two.

By using Eq. (1), the far field radiated by the reflectarray element is obtained in spherical coordinates in the Reflectarray Coordinate System (RaCS), defined by the unit vectors $(\hat{x}_r, \hat{y}_r, \hat{z}_r)$, see Figure 2. However, we are interested in obtaining the near field in Cartesian coordinates referred to the Global Coordinate System (GCS), $(\hat{x}, \hat{y}, \hat{z})$. In particular, for the quiet zone characterization, the near field is computed in planes perpendicular to $\hat{z}_a$, which is parallel to $\hat{z}$, and corresponds to the collimating direction. In order to accomplish this task, the following steps should be followed:

(i) Perform a change of coordinates of the grid point from the GCS to the RaCS applying a rotation of $\theta_0$ around $\hat{y}_r$ axis (see Figure 2) using the matrix:

$$\begin{pmatrix} x' \\ y' \\ z' \end{pmatrix} = \begin{pmatrix} \cos\theta_0 & 0 & \sin\theta_0 \\ 0 & 1 & 0 \\ -\sin\theta_0 & 0 & \cos\theta_0 \end{pmatrix} \begin{pmatrix} x \\ y \\ z \end{pmatrix}, \tag{3}$$

where $(x,y,z)$ are the grid point coordinates in the GCS and $(x',y',z')$ in the RaCS.

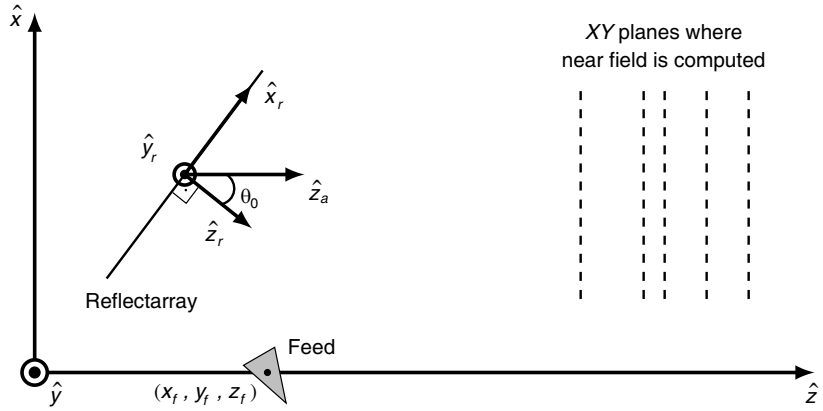


**Figure 2.** Diagram of reflectarray geometry with planes perpendicular to the collimating direction where the near field will be computed.

(ii) After computing the far field radiated by the element at a point in the RaCS using (1), perform a change of coordinates from spherical to Cartesian.

(iii) Add contributions from all reflectarray elements, computing them following steps (i) and (ii).

(iv) Perform a change of coordinates from the RaCS to the GCS using the transpose matrix employed in step (i).

This way, the near field is computed in one point in space. Steps (i)–(iv) are repeated to compute the near field in all desired points, in general in a volume. Finally, computations can be easily sped up parallelizing the process by dividing all the points among all available CPU units. This is possible since the computation of the near field at one point in space is independent from the rest.

## 3. NEAR FIELD SYNTHESIS

### 3.1. Algorithm for Quiet Zone Optimization

The chosen algorithm for the optimization of the quiet zone is the Levenberg-Marquardt Algorithm (LMA). In particular, the efficient and scalable implementation presented in [27] is used here but adapted to the near field employing the model presented in the previous section. To adapt the LMA to perform the optimization of the quiet zone, the new cost function has to reflect that now the near field is synthesized in both amplitude and phase. Thus, the cost function for general near field synthesis is

$$F^{X/Y} = \sum_{i=1}^{N_z} \left( \sum_{t=1}^{T} \left( F_{i,t,\mathrm{amp}}^{X/Y} \right)^2 + \sum_{t=1}^{T} \left( F_{i,t,\mathrm{pha}}^{X/Y} \right)^2 \right), \tag{4}$$

where $F$ is the total error, $X/Y$ the polarization of the field which is currently optimized, $N_z$ the number of near field planes, $T$ the number of points in which each near field plane is discretized, and $F_{i,t}$ the residual, defined for the near field amplitude or phase as

$$\begin{aligned} F_{i,t}^{X/Y} \;=\; & W(\vec{r}_t) \Bigg[ \left( T_U^2(\vec{r}_{i,t}) - \left| F_{x/y}^{X/Y}(\vec{r}_{i,t}) \right|^2 \right) \left( T_L^2(\vec{r}_{i,t}) - \left| F_{x/y}^{X/Y}(\vec{r}_{i,t}) \right|^2 \right) \\ & + \left| T_U^2(\vec{r}_{i,t}) - \left| F_{x/y}^{X/Y}(\vec{r}_{i,t}) \right|^2 \right| \cdot \left| T_L^2(\vec{r}_{i,t}) - \left| F_{x/y}^{X/Y}(\vec{r}_{i,t}) \right|^2 \right| \Bigg], \end{aligned} \tag{5}$$

where $\vec{r}_{i,t} = (x, y)_{i,t}$ is a point in a near field plane $i$; $W$ is a weighting function; $T_L$ and $T_U$ are the lower and upper specification templates, respectively; and $F_{x/y}^{X/Y}$ can be either the amplitude or phase residual, for either polarization depending on the superscript and either field component referred to the RaCS depending on the subscript. Note that Eq. (5) employs the squared absolute value of the

amplitude and phase, which may cause that the field would not be distinguishable from its complex conjugate. In order to solve this ambiguity, the phase should be set in the range $[0, 2\pi]$ for the residual, so the error produced by the conjugated field is not the same as the required field (which would be the case when setting the phase in the range $[-\pi, \pi]$). Also, since a POS is performed, only $F_x^X$ or $F_y^Y$ are considered, which correspond to the desired component for a given polarization.

### 3.2. Antenna Specifications and Starting Point

The considered reflectarray is the same as the one specified in a previous section working at 20 GHz. For the near field synthesis, the feed horn is modeled with a $\cos^q \theta$ function, with $q = 8.2$ which imposes an illumination taper of $-7.4$ dB at the reflectarray edges, although the real incident field could be used since the algorithm is independent of the feed model. The total size of the reflectarray surface is $180 \times 180\,\text{mm}^2$, with a projected aperture $D_x = 180\,\text{mm} \cdot \cos\theta_0 = 169\,\text{mm} = 11.27\lambda$ in the $\hat{x}$ axis and $D_y = 180\,\text{mm} = 12\lambda$ in the $\hat{y}$ axis.

As starting point for the optimization, the reflectarray collimates the field in the $\hat{z}$ direction with a radiation angle $\theta_0 = 20°$ (see Figure 2). The size of the quiet zone will be strongly limited in amplitude due to the illumination taper imposed by the feed. Hence, to facilitate convergence of the algorithm, the amplitude template will be set for a ripple of 1.25 dB and the phase template for a ripple of 10°, both in a grid defined in a circle of radius 45 mm ($3\lambda$). The optimization will be carried out in two different planes, placed at $20\lambda$ and $26.67\lambda$ from the reflectarray center. Also, it will be only carried out for $X$ polarization and the weighting function is set to $W = 1$.

### 3.3. Results

Figure 3 shows the main cut in $x$ and $z = 20\lambda$ where the amplitude has maximum value in amplitude and phase comparing the initial and optimized near field. As it can be seen, the amplitude is effectively flattened and now it complies with the specifications in the cut, while the phase ripple is reduced. Moreover, the upper specification template $T_U$ controls the maximum level of the near field outside the region of interest, which otherwise could yield relative values greater than those obtained in the coverage zone. In addition, the model previously presented is compared with simulations of the commercially available software GRASP obtaining good agreement and validating the model. The near field synthesis

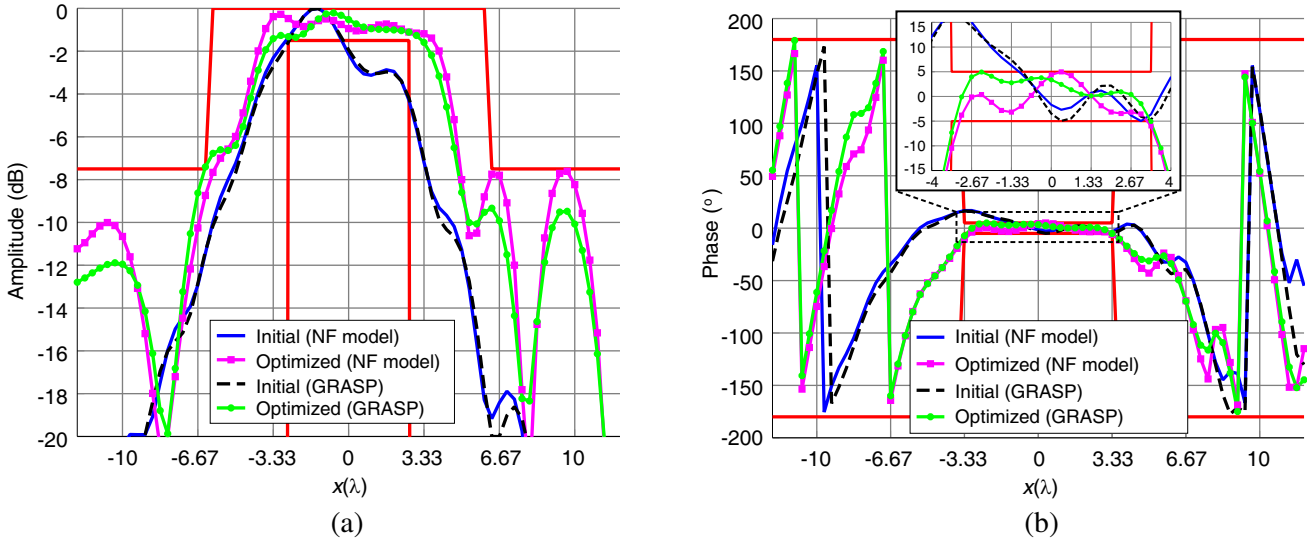


**Figure 3.** Main cut in $x$ and $z = 20\lambda$ where the amplitude has maximum value in (a) amplitude and (b) phase comparing the starting and optimized near field computed with the presented model and commercial software GRASP.

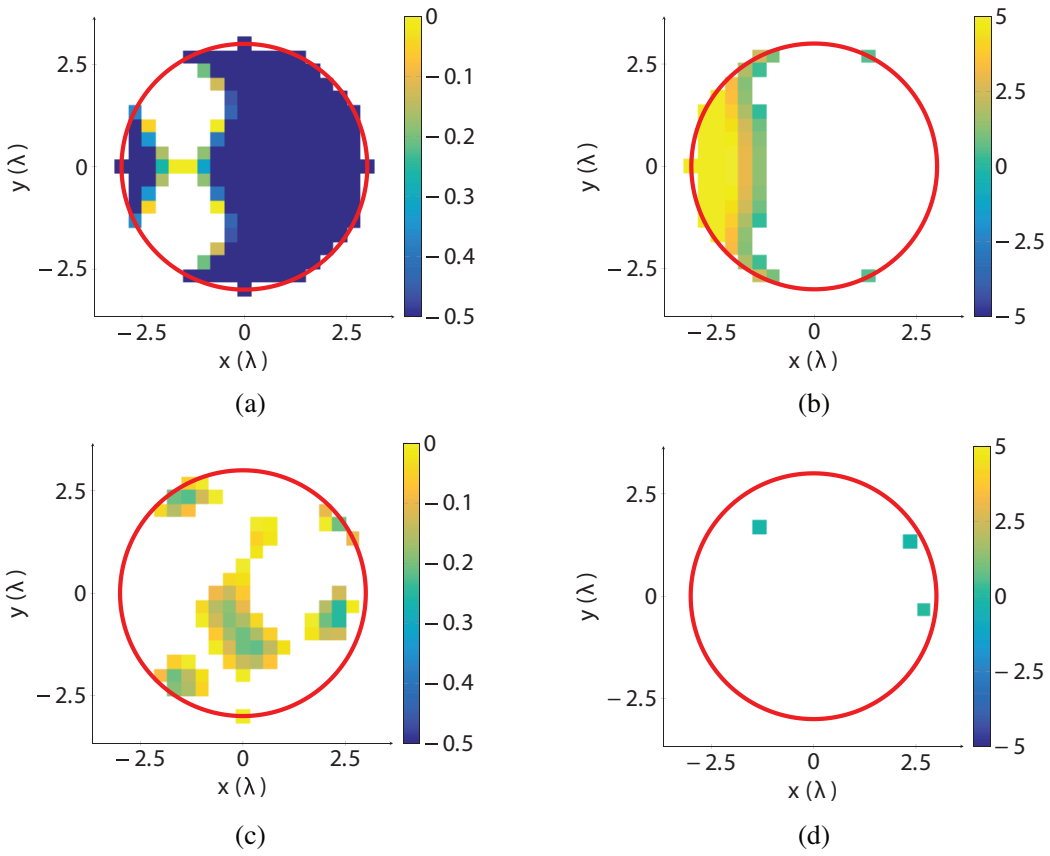


**Figure 4.** Color maps for (a), (c) amplitudes and (b), (d) phases for the plane $z = 20\lambda$, showing the (a), (b) initial and (c), (d) optimized field. The color maps represent how many dB (°) the amplitude (phase) value is to the closest template, and is white when the field complies. Red line shows the area where the ripple was imposed (1 dB or 10°), as reference.

was carried out with the near field model previously presented and GRASP is only used in analysis to validate it.

Although the reflectarray was optimized at two different near field planes ($z = 20\lambda, 26.67\lambda$), the near field was simulated in three extra planes between them to analyze the generated quiet zone in a volume. Those planes are $z = 21.67\lambda, 23.33\lambda, 25\lambda$. Figure 4 shows the results for the worse cases in amplitude and phase. The color map represents, for each point, how many dB (°) the amplitude (phase) value is to the closest template point, and is white if the field lies within bounds. For the amplitude, although the synthesis was carried out with an allowable ripple of 1.25 dB, the results shown in Figure 4 were generated using a template with an amplitude ripple of just 1 dB. Due to the strong taper imposed by the feed, the initial planes do not comply in many points, but after the optimization the improvement is patent.

Table 1 shows the compliance in per cent for the five planes in amplitude and phase for different ripples for the initial and optimized fields. As it can be seen, after the optimization, the near field surface which complies with the requirements is substantially increased. The worse case corresponds to the plane $z = 20\lambda$ with a ripple of 1 dB, complying only the 72.7% of the surface and shown in Figure 4. However, even in that case, the error is quite low, since the mean error for all the points which do not comply is of only 0.1 dB. For the rest of the planes, the phase complies in the entire coverage zone even for a ripple of 8°, while the amplitude complies in more than 90% of the surface with a ripple of 1 dB or better.

Finally, simulations were carried out in an Intel Core i3-2100, where GRASP took 15 seconds to simulate each near field plane.

**Table 1.** Compliance for different planes for amplitude and phase. Data shows percentage of surface where the ripple was allowed.

| | Amplitude | | | | Phase | | | |
|---|---|---|---|---|---|---|---|---|
| | 1.25 dB | | 1 dB | | 10° | | 8° | |
| $z(\lambda)$ | Ini. | Opt. | Ini. | Opt. | Ini. | Opt. | Ini. | Opt. |
| 20 | 27.7 | 100 | 22.1 | 72.7 | 73.9 | 98.8 | 62.8 | 93.7 |
| 21.67 | 30.0 | 99.6 | 26.1 | 96.4 | 67.6 | 100 | 56.5 | 100 |
| 23.33 | 36.4 | 98.8 | 30.0 | 92.9 | 37.9 | 100 | 32.4 | 100 |
| 25 | 48.2 | 99.6 | 40.7 | 94.5 | 29.6 | 100 | 22.1 | 100 |
| 26.67 | 56.1 | 100 | 48.6 | 98.4 | 22.5 | 100 | 18.6 | 100 |

### 3.4. Other Applications

Due to the generality of the proposed framework for general near field optimization, in which the specifications are given in form of maximum and minimum templates, and in which both the amplitude and phase of the near field are taken into account, the proposed technique may be used for other near field applications, such as RFID [11], imaging [12], microwave virus sanitizer [13] or multi-focusing [20], by adapting the cost function (for instance, setting the phase cost to zero if the near field phase does not play a role) and providing suitable templates.

Furthermore, the LMA employed in this work may be easily adapted to far field applications, by employing an array far field model instead of a near field one. This way, by giving the far field specifications by means of templates and a suitable starting point for the optimization, far field synthesis may be carried out, for applications such as monopulse radar [31], where both sum and difference patterns are needed; wireless communications [6] with LMDS specifications, having a squared cosecant pattern in elevation and sectorial in azimuth; etc. Again, a suitable starting point is important to obtain good results since the LMA is a local optimizer. For instance, in [6] the starting point is obtained using an analytical technique [32], which produces a radiation pattern which is close to meet the requirements, and then it is refined using an optimization algorithm. For monopulse radar, in [31] a power pattern synthesis with centrosymmetric layout constraints is employed using a linear programming approach, guaranteeing optimal solution. Then, the LMA could be used to further refine the results without layout constraints, which provides more degrees of freedom.

## 4. CONCLUSION

A reflectarray model for the computation of its near field has been presented with the aim of characterizing and improving the quiet zone generated by the antenna. The model computes the near field of the whole antenna as the far field contribution of all elements of the reflectarray considering them small rectangular apertures and thus taking into account the active element pattern. The reflectarray near field model was then used to perform a synthesis of the complex near field, considering both amplitude and phase, to employ the reflectarray as a probe for Compact Antenna Test Range (CATR) applications. The goal is to optimize the quiet zone generated by the reflectarray, imposing certain constraints in the amplitude and phase ripple, while also controlling the near field outside the area of interest. Due to the strong amplitude illumination taper imposed by the feed, the size of the quiet zone is strongly limited. Two near field planes were considered in the synthesis. After the optimization, the size of the quiet zone was greatly improved. Three more intermediate near field planes were simulated before and after the optimization and the quiet zone improvement in all of them was patent. In fact, even for the worse case (amplitude with an allowed ripple of 1 dB), the mean error in the points which do not comply is only 0.1 dB. These results demonstrate that reflectarrays could be a potential substitute for parabolic reflectors in CATR applications, specially at high frequencies above 100 GHz and up to 200 GHz, given the current precision in the manufacturing process.

## ACKNOWLEDGMENT

This work was supported in part by the European Space Agency under Contract ESTEC/AO/1-7064/12/NL/MH, in part by the Ministerio de Economía y Competitividad, under Project TEC2014-54005-P (MIRIIEM), in part by the Gobierno del Principado de Asturias/FEDER under Project GRUPIN14-114.

## REFERENCES

1. Huang, J. and J. A. Encinar, *Reflectarray Antennas*, John Wiley & Sons, Hoboken, NJ, USA, 2008.
2. Encinar, J. A., L. S. Datashvili, J. A. Zornoza, M. Arrebola, M. Sierra-Castaner, J. L. Besada-Sanmartin, H. Baier, and H. Legay, "Dual-polarization dual-coverage re ectarray for space applications," *IEEE Trans. Antennas Propag.*, Vol. 54, No. 10, 2827–2837, Oct. 2006.
3. Encinar, J. A., M. Arrebola, L. F. de la Fuente, and G. Toso, "A transmit-receive reflectarray antenna for direct broadcast satellite applications," *IEEE Trans. Antennas Propag.*, Vol. 59, No. 9, 3255–3264, Sep. 2011.
4. Legay, H., D. Bresciani, E. Labiole, R. Chiniard, and R. Gillard, "A multi facets composite panel re ectarray antenna for a space contoured beam antenna in Ku band," *Progress In Electromagnetics Research B*, Vol. 54, 1–26, 2013.
5. Capozzoli, A., C. Curcio, A. Liseno, and G. Toso, "Fast, phase-only synthesis of aperiodic re ectarrays using NUFFTs and CUDA," *Progress In Electromagnetics Research*, Vol. 156, 83–103, 2016.
6. Arrebola, M., J. A. Encinar, and M. Barba, "Multifed printed re ectarray with three simultaneous shaped beams for LMDS central station antenna," *IEEE Trans. Antennas Propag.*, Vol. 56, No. 6, 1518–1527, Jun. 2008.
7. Yu, J.-F., L. Chen, J. Yang, and X.-W. Shi, "An improved predesign procedure for shaped-beam re ectarrays," *Progress In Electromagnetics Research M*, Vol. 40, 119–127, 2014.
8. Zornoza, J. A., R. Leberer, J. A. Encinar, and W. Menzel, "Folded multilayer microstrip re ectarray with shaped pattern," *IEEE Trans. Antennas Propag.*, Vol. 54, No. 2, 510–518, Feb. 2006.
9. Rengarajan, S. R., "Reflectarrays of rectangular microstrip patches for dual-polarization dual-beam radar interferometers," *Progress In Electromagnetics Research*, Vol. 133, 1–15, 2013.
10. Patyuchenko, A., C. Tienda, M. Younis, S. Bertl, P. Lopez-Dekker, and G. Krieger, "Digital beamforming SAR interferometer based on a multi-beam re ectarray antenna," *Proceedings of the 10th European Conference on Synthetic Aperture Radar (EUSAR)*, 1–4, Berlin, Germany, Jun. 3–5, 2014.
11. You, B.-Q., Y.-X. Liu, J.-H. Zhou, and H.-T. Chou, "Numerical synthesis of dual-band reflectarray antenna for optimum near-field radiation," *IEEE Antennas Wireless Propag. Lett.*, Vol. 11, 760–762, 2012.
12. Kamoda, H., T. Iwasaki, J. Tsumochi, T. Kuki, and O. Hashimoto, "60-GHz electronically reconfigurable large re ectarray using single-bit phase shifters," *IEEE Trans. Antennas Propag.*, Vol. 59, No. 7, 2524–2531, Jul. 2011.
13. Hung, W.-T., J.-J. Tung, and S.-Y. Chen, "A focusing re ectarray and its application in microwave virus sanitizer," *Radio Sci.*, Vol. 49, No. 10, 890–898, Oct. 2014.
14. Olver, A. D., "Compact antenna test ranges," *Seventh International Conference on Antennas and Propagation (ICAP)*, 99–108, York, UK, Apr. 15–18, 1991.
15. Karttunen, A., J. Ala-Laurinaho, M. Vaaja, T. Koskinen, J. Häkli, A. Lönnqvist, J. Mallat, A. Tamminen, V. Viikari, and A. V. Räisänen, "Antenna tests with a hologram-based CATR at 650 GHz," *IEEE Trans. Antennas Propag.*, Vol. 57, No. 3, 711–720, Mar. 2009.
16. Hu, W., M. Arrebola, R. Cahill, J. A. Encinar, V. Fusco, H. S. Gamble, Y. Álvarez, and F. Las-Heras, "94 GHz dual-reflector antenna with re ectarray subreflector," *IEEE Trans. Antennas Propag.*, Vol. 57, No. 10, 3043–3050, Oct. 2009.

17. Prado, D. R., M. Arrebola, M. R. Pino, and F. Las-Heras, "Evaluation of the quiet zone generated by a re ectarray antenna," *International Conference on Electromagnetics in Advanced Applications (ICEAA)*, 702–705, Cape Town, South Africa, Sep. 2–7, 2012.
18. Vaquero, A. F., D. R. Prado, M. Arrebola, M. R. Pino, and F. Las-Heras, "Near field synthesis of re ectarrays using intersection approach," *11th European Conference on Antennas and Propagation (EuCAP)*, 3644–3648, Paris, France, Mar. 19–24, 2017.
19. Vaquero, A. F., D. R. Prado, M. Arrebola, M. R. Pino, and F. Las-Heras, "Reflectarray probe optimization at millimeter frequencies," *10th European Conference on Antennas and Propagation (EuCAP)*, 1–5, Davos, Switzerland, Apr. 10–15, 2016.
20. Álvarez, J., R. G. Ayestarán, G. León, L. F. Herrán, A. Arboleya, J. A. López-Fernández, and F. Las-Heras, "Near field multifocusing on antenna arrays via non-convex optimisation," *IET Microw. Antennas Propag.*, Vol. 8, No. 10, 754–764, Jul. 2014.
21. Ismail, T. H., D. I. Abu-Al-Nadi, and M. J. Mismar, "Phase-only control for antenna pattern synthesis of linear arrays using the Levenberg-Marquardt algorithm," *Electromagnetics*, Vol. 24, No. 7, 555–564, 2004.
22. Nocedal, J. and S. J. Wright, *Numerical Optimization*, 2nd Edition, Springer, New York, NY, USA, 2006.
23. Aghasi, A., H. Amindavar, E. L. Miller, and J. Rashed-Mohassel, "Flat-top footprint pattern synthesis through the design of arbitrary planar-shaped apertures," *IEEE Trans. Antennas Propag.*, Vol. 58, No. 8, 2539–2552, Aug. 2010.
24. Wen, Y., W. S. Gan, and J. Yang, "Nonlinear least-square solution to at-top pattern synthesis using arbitrary linear array," *Signal Process.*, Vol. 85, No. 9, 1869–1874, Sep. 2005.
25. Álvarez, J., R. G. Ayestarán, and F. Las-Heras, "Design of antenna arrays for near-field focusing requirements using optimisation," *Electron. Lett.*, Vol. 48, No. 21, 1323–1325, Oct. 2012.
26. Álvarez, J., M. Arrebola, R. G. Ayestarán, and F. Las-Heras, "Systematic framework for re ectarray synthesis based on phase optimization," *Int. J. Antennas Propag.*, Vol. 2012, 1–9, Jun. 2012.
27. Prado, D. R., J. Álvarez, M. Arrebola, M. R. Pino, R. G. Ayestarán, and F. Las-Heras, "Efficient, accurate and scalable re ectarray phase-only synthesis based on the Levenberg-Marquardt algorithm," *Appl. Comp. Electro. Society Journal*, Vol. 30, No. 12, 1246–1255, Dec. 2015.
28. Encinar, J. A. and M. Barba, "Design manufacture and test of Ka-band reflectarray antenna for trasmitting and receiving in orthogonal polarization," *14th International Symposium on Antenna Technology and Applied Electromagnetics*, 1–4, Ottawa, Canada, Jul. 5–8, 2010.
29. Arboleya, A., Y. Alvarez, and F. Las-Heras, "Millimeter and submillimeter planar measurement setup," *IEEE Antennas and Propagation Society International Symposium (APSURSI)*, 1–2, Orlando, Florida, USA, Jul. 7–13, 2013.
30. Rahmat-Samii, Y., L. I. Williams, and R. G. Yaccarino, "The UCLA bi-polar planar-near-field antenna-measurement and diagnostics range," *IEEE Antennas Propag. Mag.*, Vol. 37, No. 6, 16–35, Dec. 1995.
31. Rocca, P. and A. F. Morabito, "Optimal synthesis of reconfigurable planar arrays with simplified architectures for monopulse radar applications," *IEEE Trans. Antennas Propag.*, Vol. 63, No. 3, 1048–1058, Mar. 2015.
32. Chakraborty, A., B. N. Das, and G. S. Sanyal, "Beam shaping using nonlinear phase distribution in a uniformly spaced array," *IEEE Trans. Antennas Propag.*, Vol. 30, No. 5, 1031–1034, Sep. 1982.